Molecular Therapy
Methods & Clinical Development
Original Article

ISPD Overexpression Enhances Ribitol-Induced Glycosylation of α-Dystroglycan in Dystrophic FKRP Mutant Mice

Marcela P. Cataldi,[1] Anthony Blaeser,[1] Peijuan Lu,[1] Victoria Leroy,[1] and Qi Long Lu[1]

[1]McColl-Lockwood Laboratory for Muscular Dystrophy Research, Cannon Research Center, Carolinas Medical Center, Atrium Health, Charlotte, NC 28203, USA

Dystroglycanopathy, a subgroup of muscular dystrophies, is characterized by hypoglycosylation of α-dystroglycan (α-DG), which reduces its laminin-binding activity to extracellular matrix proteins, causing progressive loss of muscle integrity and function. Mutations in the fukutin-related protein (FKRP) gene are the most common causes of dystroglycanopathy. FKRP transfers ribitol-5-phosphate to the *O*-mannosyl glycan on α-DG from substrate cytidine diphosphate (CDP)-ribitol, which is synthesized by isoprenoid synthase domain-containing protein (ISPD). We previously reported that oral administration of ribitol restores therapeutic levels of functional glycosylation of α-DG (F-α-DG) in a FKRP mutant mouse model. Here we examine the contribution of adeno-associated virus (AAV)-mediated overexpression of ISPD to the levels of CDP-ribitol and F-α-DG with and without ribitol supplementation in the disease model. ISPD overexpression alone and in combination with ribitol improves dystrophic phenotype. Furthermore, the combined approach of ribitol and ISPD acts synergistically, increasing F-α-DG up to 40% of normal levels in cardiac muscle and more than 20% in limb and diaphragm. The results suggest that low levels of substrate limit production of CDP-ribitol, and endogenous ISPD also becomes a limiting factor in the presence of a supraphysiological concentration of ribitol. Our data support further investigation of the regulatory pathway for enhancing efficacy of ribitol supplement to FKRP-related dystroglycanopathy.

INTRODUCTION

Muscular dystrophies are genetic diseases characterized with progressive muscle weakness and wasting. The diseases are heterogeneous in causes and in clinical manifestation, and have been classified into different subgroups according to genes affected, biochemical features, and/or severity. Dystroglycanopathies (referred to as muscular dystrophy-dystroglycanopathies [MDDGs]) are a form of muscular dystrophy specifically caused by mutations in genes involved in the synthesis of the glycan chain on the α subunit of dystroglycan (α-DG) and are characterized by reduced to absence of functional glycosylation of α-DG (F-α-DG).[1] α-DG is a peripheral membrane protein extensively glycosylated with both *N*-linked and *O*-linked glycans. The *O*-mannosylated glycan on α-DG acts as a cellular receptor for laminin and other extracellular matrix (ECM) proteins, including agrin, perlecan, neurexin, and pikachurin.[2–6] The interaction of α-DG with ECM proteins is critical for maintaining muscle integrity.[7] To date, mutations in at least 18 different genes have been associated with hypoglycosylation of α-DG. Among them, mutations in the gene encoding for the fukutin-related protein (FKRP) are the most common causes of dystroglycanopathy. The disease presents a wide spectrum of clinical severity ranging from mild limb girdle muscular dystrophy (LGMD) 2I (also referred to as MDDG type C) without compromise of central nervous system, to severe congenital muscular dystrophy (MDDG type A), Walker-Warburg syndrome (WWS), and muscle-eye-brain disease (MEB).[8–10] An intermediate form (MDDG type B) with or without mental retardation has also been described.[11,12] The severe forms of the disease can cause developmental delay and mental retardation. In FKRP-related dystroglycanopathies, reduced or lack of F-α-DG results in progressive degeneration of skeletal and cardiac muscles. As a result, patients gradually lose mobility with impaired and ultimately failure of respiratory and cardiac functions.[13] Currently, no treatment is available, although several experimental therapies are being tested pre-clinically.[14–16]

Recently, the enzymatic action of FKRP and fukutin (FKTN) has been identified as ribitol-5-phosphate (ribitol-5P) transferase, adding a tandem ribitol-5P structure to CoreM3 [GalNAc-β1-3GlcNAc-β1-4(P-6) Man-1-Thr/Ser] of α-DG.[17,18] Furthermore, both transferases have been demonstrated to use cytidine diphosphate ribitol (CDP-ribitol) as substrate, which is synthesized by isoprenoid synthase domain-containing protein (ISPD) (recently renamed as CDP-L-ribitol pyrophosphorylase A [CRPPA]).[17–20] Mutations in ISPD have been implicated in WWS, the severe forms of dystroglycanopathies (MDDGA7), and in a less severe form of LGMD without brain and eye anomalies (MDDGC7).[21–24]

A study from Gerin et al.[18] demonstrated that overexpression of ISPD increased ribitol incorporation into α-DG in wild-type cells *in vitro*,

Received 18 July 2019; accepted 3 December 2019;
https://doi.org/10.1016/j.omtm.2019.12.005.

Correspondence: Qi Long Lu, McColl-Lockwood Laboratory for Muscular Dystrophy Research, Cannon Research Center, Carolinas Medical Center, Atrium Health, Charlotte, NC 28203, USA.
E-mail: qi.lu@atriumhealth.org

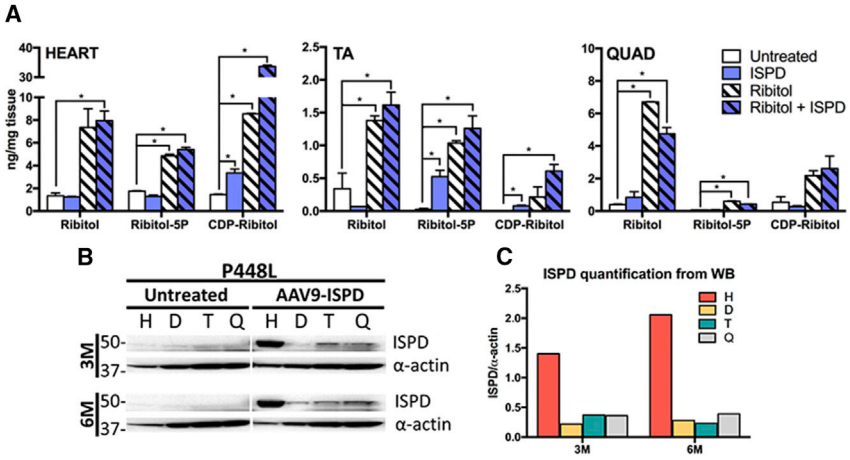

Figure 1. Quantification of Metabolites and Exogenous ISPD

(A) Quantification of ribitol, ribitol-5P, and CDP-ribitol levels by LC/MS-MS from heart, tibialis anterior (TA), and quadriceps (QUADs) of 19-week-old P448L mice either untreated or treated with a single injection of 5e13 vg/kg AAV9-ISPD (ISPD), supplementation of 5% ribitol in drinking water (Ribitol), or both treatments combined (Ribitol + ISPD) (n = 2 per each cohort). Error bars represent mean ± SEM. Unpaired t test, *$p \leq 0.05$. (B) Western blot from heart (H), diaphragm (D), tibialis anterior (T), and quadricep (Q) of untreated mice or mice injected with 5e13vg/g AAV9-ISPD, collected at 3 months (3M) or 6 months (6M) post-injection. Detection of α-actin was used as loading control. (C) Quantification of ISPD band intensity from samples treated with AAV9-ISPD from western blot in (B). Values were normalized to α-actin expression for each tissue.

suggesting that the levels of CDP-ribitol might be a limiting factor for F-α-DG. Moreover, we have recently reported that orally administered ribitol is converted to CDP-ribitol in cardiac and skeletal muscle of the FKRP mouse model containing a P448L mutation (P448L), and that the increased levels of CDP-ribitol enhance the levels of F-α-DG in muscles.[25] We therefore hypothesized that enhanced expression of ISPD could increase conversion of ribitol into CDP-ribitol, thus potentially enhancing FKRP-mediated transfer of ribitol-5P to the core glycan chain of α-DG and, consequently, restoring F-α-DG in muscles with partial FKRP deficiency. In the current study, we investigate the implication of AAV-mediated ISPD overexpression, alone and in combination with ribitol supplementation, on levels of CDP-ribitol and F-α-DG in the P448L FKRP mutant mouse model.

Our results demonstrate that overexpression of ISPD increases the tissue levels of CDP-ribitol and F-α-DG. Moreover, the combined treatment of ISPD and ribitol synergistically increases the pool of CDP-ribitol in muscles, especially in cardiac muscle of P448L FKRP mutant mice, resulting in the synthesis of F-α-DG up to 40% of normal levels in cardiac muscle and more than 20% in limb and diaphragm. However, the results also raise the question of potential side effects with ISPD overexpression.

RESULTS

AAV-Mediated Overexpression of ISPD Increases Levels of CDP-Ribitol in FKRP Mutant Mice

We have previously reported that orally administered ribitol is converted to ribitol-5P and CDP-ribitol in cardiac and skeletal muscle of the P448L FKRP mutant mouse model. Moreover, the increased levels of CDP-ribitol are associated with a higher rate of ribitol-5P incorporation to α-DG by the mutant FKRP. To investigate the contribution of ISPD to the levels of CDP-ribitol converted from endogenous and exogenous ribitol, and its impact on levels of F-α-DG, we overexpressed ISPD systemically with a single tail-vein injection of 5e13 vg/kg (vector genome per kilogram of body weight) adeno-associated virus serotype 9 (AAV9) carrying a human ISPD coding sequence under control of a cytomegalovirus (CMV) promoter (AAV9-ISPD). Mice were injected at 5 weeks of age, an early stage in disease progression, and 5% ribitol treatment began 10 days post-injection. The animals drinking water only were used as control. Three metabolites, ribitol, ribitol-5P and CDP-ribitol, were measured and quantified by liquid chromatography with tandem mass spectrometry (LC/MS-MS) in heart, tibialis anterior, and quadriceps tissues from mice treated for 3 months. As expected, overexpression of ISPD alone had no effect on ribitol levels (Figure 1). In contrast, the level of ribitol was significantly increased in the tissues of mice drinking ribitol. Levels of CDP-ribitol significantly increased in heart of both ribitol- and ISPD-treated cohorts, with a more pronounced increase when the two treatments were combined. CDP-ribitol levels in heart were increased by 2-fold, 6-fold, and 24-fold with overexpression of ISPD, 5% ribitol, or combined treatments, respectively. This result supports our hypothesis that in the presence of exogenous ribitol, the endogenous level of ISPD expression could also become a limiting factor for the conversion of ribitol to CDP-ribitol. The increased level of CDP-ribitol in the tibialis anterior and quadriceps of the AAV9-ISPD-treated animals, either in the presence or absence of supplemented ribitol, was not as pronounced as in heart (Figure 1A). This is likely due to the fact that AAV9 transduces cardiac tissue more efficiently than skeletal muscles.[26] We therefore measured levels of exogenous ISPD expression by western blot with an antibody targeting the FLAG tag fused to the carboxyl terminus of the open reading frame (ORF) in the AAV9 vector (Figures 1B and 1C). Consistently, the levels of exogenous ISPD expression were considerably higher in heart than in diaphragm, tibialis anterior, and quadricep, either at 3 or 6 months post-injection.

Ribitol Supplementation and ISPD Overexpression Increase F-α-DG in Skeletal and Cardiac Muscle of FKRP Mutant Mice

To evaluate whether the increase in levels of CDP-ribitol correlates with enhanced glycosylation of α-DG in P448L FKRP mutant mice, we analyzed F-α-DG in heart and skeletal muscles from mice treated at two AAV9-ISPD doses of 1e13 vg/kg (low dose) and 5e13 vg/kg (high dose) with and without supplementation of 5% ribitol in drinking water. Immunohistochemistry with the monoclonal antibody

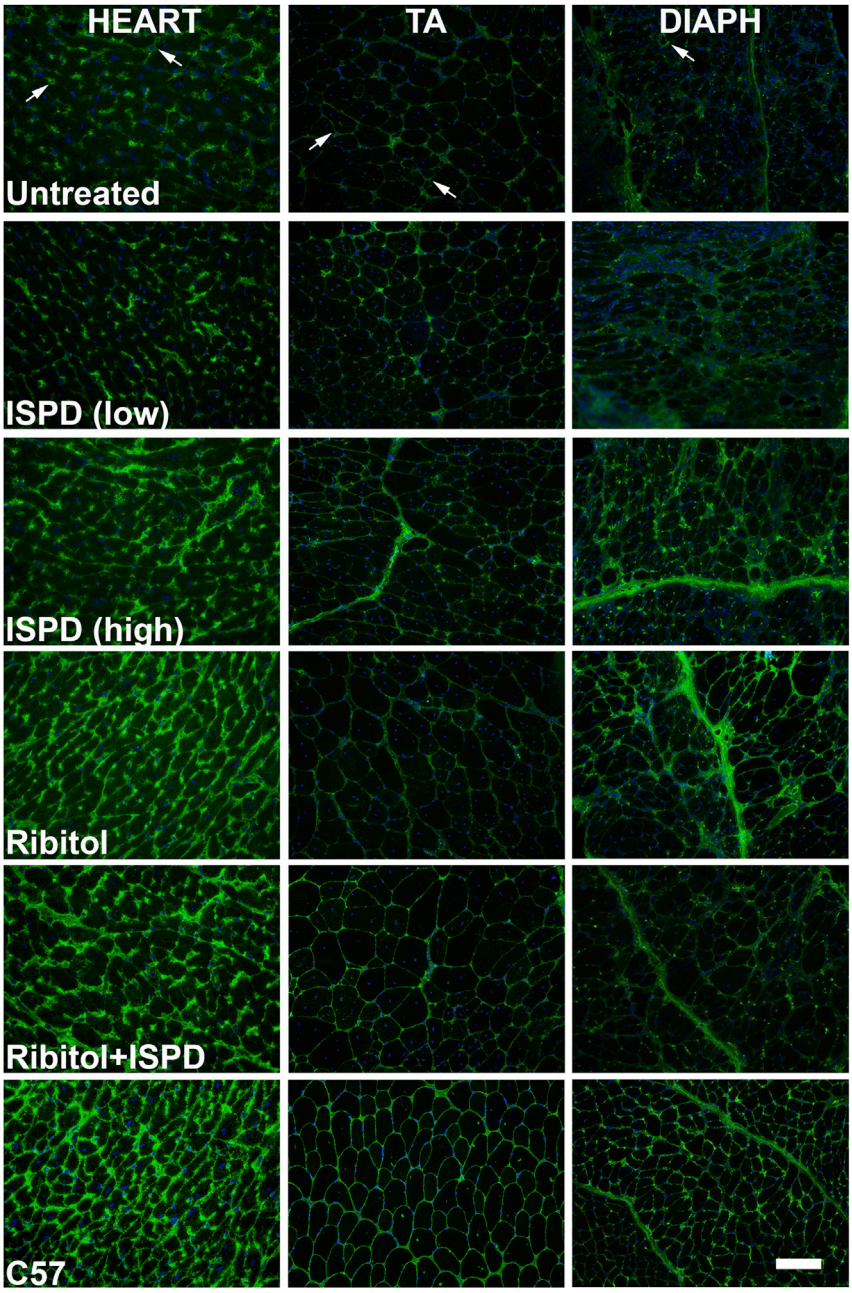

Figure 2. Rescue of F-α-DG by AAV-Mediated Overexpression of ISPD with and without Supplementation of 5% Ribitol in P448L Mice

IIH6C4 immunofluorescence staining of cardiac (heart), TA, and diaphragm (diaph) tissues from P448L mice untreated or injected with 1e13 [ISPD (low)] or 5e13 vg/kg [ISPD (high)] AAV9-ISPD. Mice drank water only or water supplemented with 5% ribitol (Ribitol). Mice of combined treatment received 5% ribitol in drinking water and a single injection of 5e13vg/kg AAV9-ISPD (Ribitol + ISPD). C57 control mice were drinking water only. All cohorts were treated for 6 months and compared with age-matched untreated controls. Arrows indicate revertant fibers expressing detectable F-α-DG in untreated mice. Nuclei were counterstained with DAPI (blue). Scale bar, 50 μm.

IIH6C4, which specifically recognizes the laminin-binding epitope of F-α-DG, showed that overexpression of ISPD from the low dose of AAV9-ISPD did not distinctively increase F-α-DG signal in all tissues examined when compared with the untreated mice. This, together with the fact that expression of exogenous ISPD was not detected in all the muscles, suggests that this low dose of AAV9-ISPD with CMV promoter was insufficient to produce the amount of ISPD required to achieve detectable enhancement in F-α-DG. Therefore, further study examined only the effect of high-dose AAV9-ISPD. In contrast, high-dose AAV9-ISPD clearly increased levels of F-α-DG in the skeletal muscle. The enhancement was more evident in the heart tissue, although the signal was patchy and significantly weaker when compared with the same tissue of C57 control mice (Figure 2). A more intense and homogeneous F-α-DG signal was detected in heart, diaphragm, and limb muscles from the mice drinking ribitol alone compared with the mice expressing exogenous ISPD. Importantly, the cohort that received the combined treatment with high-dose AAV9-ISPD and ribitol showed the strongest levels of F-α-DG. Nearly all fibers in the cardiac tissue, as well as most fibers in both diaphragm and limb muscle, were positive for IIH6C4 immunofluorescence. In contrast, F-α-DG was undetectable in cardiac and skeletal muscle of the age-matched untreated P448L control mice given drinking water only, except for a few isolated revertant fibers (Figure 2). The different levels of enhancement of F-α-DG were further confirmed by western blot analysis with the same antibody and laminin overlay assay, reaching up to 5%, 17%, and 38% of normal levels in the cardiac muscle of the cohort overexpressing ISPD, ribitol treated, and with combined treatment, respectively (Figures 3A and 3B). The highest level of F-α-DG expression was also observed in limb muscle and diaphragm of mice receiving combined treatment, reaching up to 24% and 32% of normal levels, respectively. Altogether, these data suggest that overexpression of ISPD increases CDP-ribitol substrate levels and further enhances ribitol-mediated restoration of F-α-DG in P448L FKRP mutant. However, such a correlation may not be linear because other unknown factors could also affect substrate and enzyme interaction.

To assess whether the increase in F-α-DG might also be contributed by a positive feedback effect on the expression levels of FKRP triggered by exogenous ribitol supplementation and supraphysiological

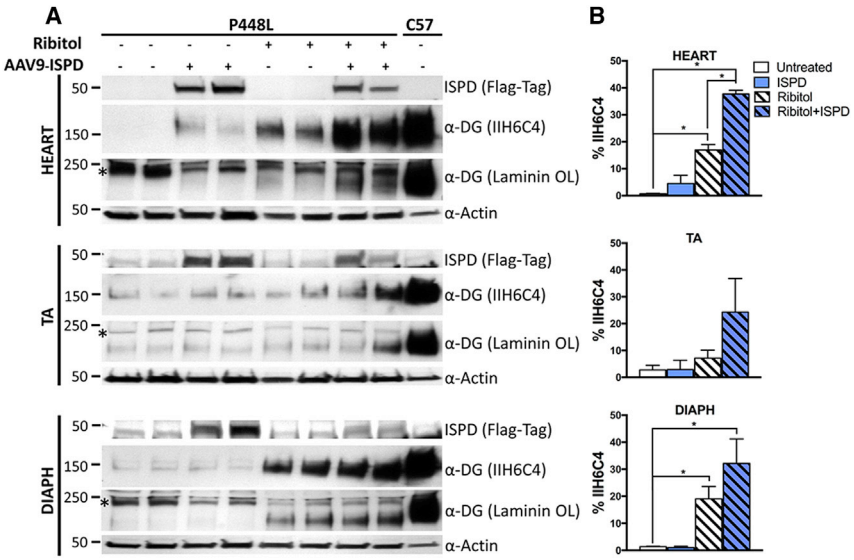

Figure 3. Rescue of F-α-DG by ISPD Overexpression with and without Ribitol Supplementation in P448L Mice Treated for 6 Months

(A) Western blot and laminin overlay assay of lysates from heart, TA, and diaph of untreated mice, mice injected with 5e13 vg/kg AAV9-ISPD, mice drinking water with 5% ribitol, and mice co-treated with 5e13 vg/kg AAV9-ISPD and drinking water with 5% ribitol (two samples are shown for each group). F-α-DG was detected by blotting with IIH6C4 and laminin overlay assay (laminin OL). Asterisks indicate the upper band in laminin OL assay is endogenous laminin present in all the samples. Expression of exogenous ISPD was detected with an anti-FLAG-Tag antibody. Detection of α-actin was used as loading control. (B) Quantification of IIH6C4 band intensity from western blot. Values were normalized to α-actin expression for each tissue and shown as percentage of C57 levels. Error bars represent mean ± SEM. Unpaired t test, *p ≤ 0.05.

concentrations of CDP-ribitol, we measured levels of mutant FKRP mRNA transcripts by quantitative real-time PCR in cardiac muscle, limb muscle, and diaphragm (Figure S1). No significant difference in levels of FKRP transcripts was observed between mice of all treated groups and the untreated control.

Administration of Ribitol and ISPD Improves Histopathology of P448L Mutant Mice

Histological improvement on the dystrophic phenotype of P448L mice treated with supplemented ribitol and/or overexpression of ISPD was demonstrated by hematoxylin and eosin (H&E) staining (Figure 4). Consistent with previous reports, large areas of degenerating fibers, with high variation in fiber sizes and high percentage of centrally nucleated fibers (CNFs), were observed in the skeletal muscles of the untreated P448L mice (Figures 4 and 5). On the other hand, as shown by the fiber size normal distribution curve, treatment with 5e13 vg/kg AAV9-ISPD and with ribitol supplementation improved the dystrophic pathology of limb muscles, evidenced by the shift of the curves toward the right (bigger fiber diameter) compared with untreated mice (Figure 5A, left panel). Quantitative analysis also showed a statistically significant decrease in the number of fibers with small diameters indicating a decrease in the process of degeneration/regeneration characteristic of dystrophic muscles (Figure 5A, right panel). However, the effect of AAV9-ISPD treatment alone was limited compared with that of ribitol, probably because of the diminishing and uneven distribution in transduction efficiency of AAV9 with CMV promoter in limb muscles.

A reduction of the percentage of CNFs was observed in tibialis anterior from mice expressing exogenous ISPD and from mice treated with ribitol compared with untreated mice. Remarkably, a statistically significant decrease was observed from mice receiving combined therapy (Figure 5).

Moreover, a significant decrease on areas of fibrotic tissue was detected by Masson's Trichrome staining on diaphragms of the treated P448L mice when compared with untreated mice (Figure 6). Quantitative analysis showed that fibrosis encompassed 40% of the tissue per cross-sectional area in diaphragms of untreated mice, and that percentage decreased to 30%, 14%, and 13% of mice with a dose of 5e13vg/kg AAV9-ISPD, drinking ribitol only, and receiving combined treatment, respectively (Figure 6B). The limited synergistic effect observed with the current combined treatment suggests that maximal benefit of a combinatorial therapy may require dose optimization of both treatments.

Effect of Ribitol and ISPD Administration on Skeletal Muscle Function

To assess the impact of different levels of F-α-DG restoration and histology improvement on skeletal muscle function, we performed a treadmill exhaustion test at 3 and 6 months post-treatment initiation (Figure 7). Mice of all treated cohorts showed improvement in running distance and time at the 3-month time point, with the mice treated with 5e13 vg/kg AAV9-ISPD running the longest distances and for the longest time, although the difference compared with untreated mice remained not statistically significant. At 6 months post-treatment, all treated cohorts presented a clear, although not statistically significant, improvement on total distance and time compared with untreated mice. Nevertheless, the potential effect of ribitol on cellular metabolism and thus muscle function remains to be explored. We also evaluated respiratory function by whole-body plethysmography (Figure S2). At 3 months post-treatment, no statistically significant changes were detected between all cohorts, although improvements were noticed in tidal volume (TV), minute volume (MV), and expired volume (EV) on AAV9-ISPD-treated mice. Unexpectedly, TV, MV, and EV, together with peak inspiratory flow (PIF), decreased in the cohort overexpressing ISPD at 6 months

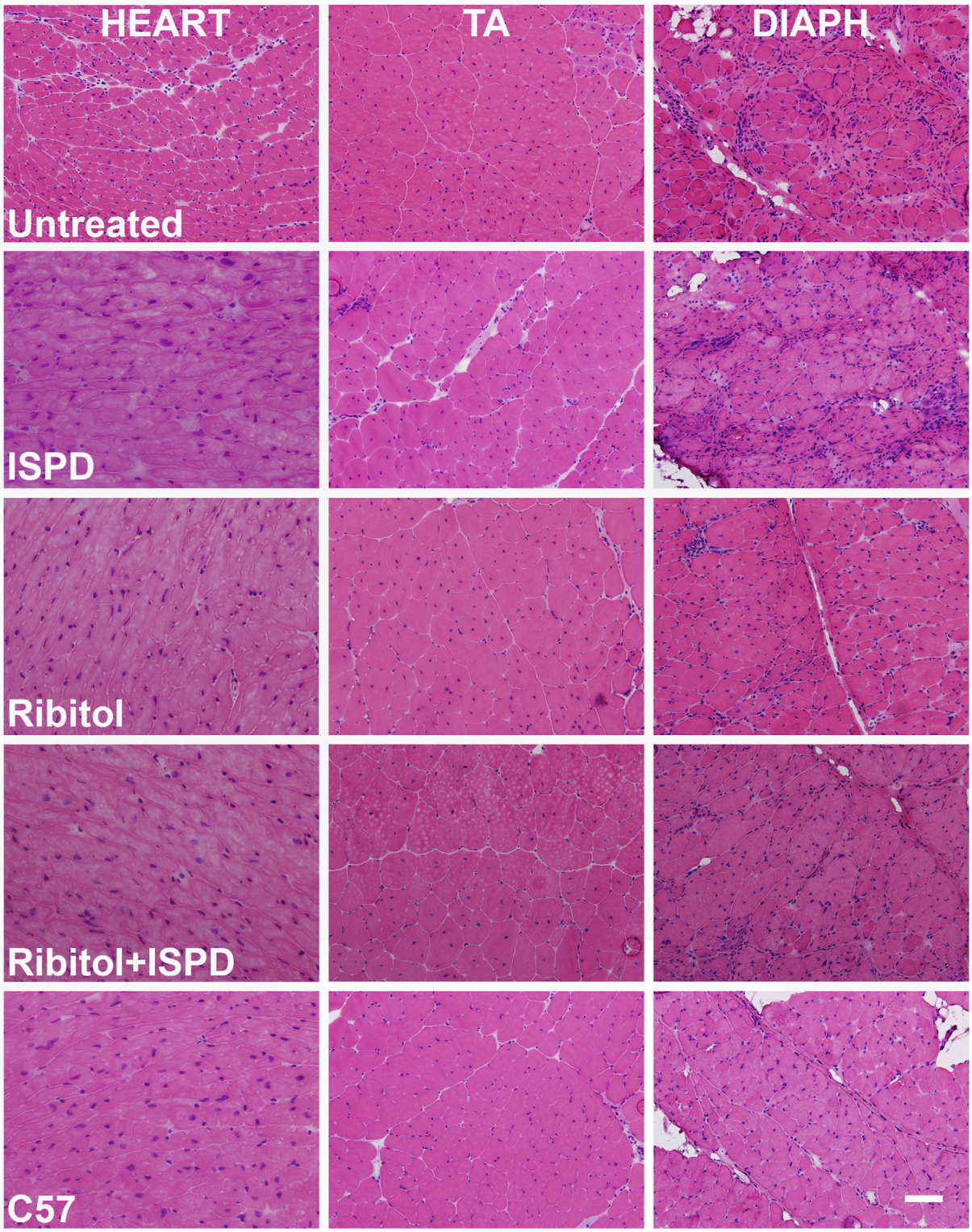

Figure 4. Histopathology of Muscle Tissues from P448L Mice Treated with Ribitol and AAV9-ISPD

H&E staining of heart, TA, and diaph tissues from control P448L mice (untreated) or mice injected with 5e13 vg/kg AAV9-ISPD (ISPD). Mice drank only water or water supplemented with 5% ribitol (Ribitol). Mice receiving combined treatment were injected with 5e13 vg/kg AAV9-ISPD and drank water supplemented with 5% ribitol (Ribitol + ISPD). Scale bar, 50 μm.

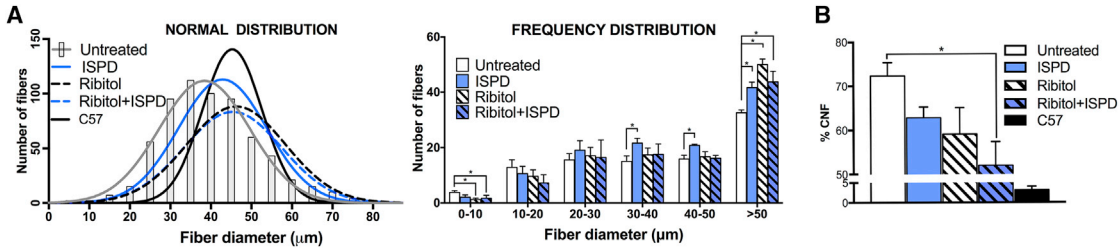

Figure 5. Quantification of the Dystrophic Phenotype Alleviation in P448L Mice Expressing Exogenous ISPD and/or Ribitol Treated

(A) Fiber size normal and frequency distribution (left and right panels, respectively) in TA muscles of either treated or untreated P448L mice and C57 control. Mice received 5e13 vg/kg AAV9-ISPD (ISPD), drank water supplemented with 5% ribitol (Ribitol), or received combined treatment (Ribitol + ISPD) for 6 months (n = 4 per each cohort). (B) Percentage of centrally nucleated fibers (CNFs) in TA muscles of P448L mice and age-matched C57 control. The same cohorts as described in (A) were analyzed (n = 4 per each cohort). Error bars represent mean ± SEM. Unpaired t test, *$p \leq 0.05$.

post-treatment compared with the untreated control, with a statistically significant difference reached for TV and PIF. Interestingly, combination with ribitol treatment appeared to mitigate the reduction of these respiratory parameters. Cohorts treated with ribitol for 3 and 6 months showed limited change in most parameters. However, one noticeable change is the shortened time of end inspiratory pause (EIP) in both ribitol-treated and combined treated cohorts at 6 months post-treatment. EIP extent is one of the most significant changes between wild-type mouse and the P448L mutant mice, and shortened time of EIP has consistently been associated with effective gene therapy reported earlier with the same FKRP mutant mouse model.[16] These data suggest that overexpression of ISPD for a prolonged period of time may affect the pattern of respiration, and ribitol treatment may limit the potentially undesirable effect of ISPD overexpression.

Ribitol-treated females and males were slightly heavier in body weight by the end of 6 months of treatment, whereas the AAV9-ISPD-treated mice showed a slight decrease in body weight (Figure S3). However, these differences were not statistically significant when compared with the age-matched untreated control mice.

DISCUSSION

Significant advances during the last few years have helped to unravel the pathway for F-α-DG synthesis by identifying the genes directly involved in the process. Most relevant, the function of FKRP has been identified as a ribitol-5P-transferase from substrate CDP-ribitol to the α-DG glycan chain, and ISPD as a cytidyltransferase synthesizing CDP-ribitol from ribitol-5P. These advances have opened new venues for experimental therapy for dystroglycanopathies with deficiency in FKRP. Indeed, recently, our group confirmed that ribitol supplementation can partially compensate for the limited function of mutant FKRP in the P448L mutant mouse model. As a result, restoration of therapeutic levels of F-α-DG and amelioration of dystroglycanopathy symptoms were achieved, making ribitol a potential new class of experimental drug for FKRP-related dystroglycanopathies. However, supplementation of ribitol alone has potential limitations, especially because lifelong treatment is required for muscular dystrophy. The levels of restored F-α-DG achieved so far are relatively low, approximately within 20% of normal levels in the mouse model. Also, importantly, the reported levels of F-α-DG with significant improvement in skeletal muscle functions are achieved with relatively high doses of ribitol, equivalent to up to 5 and 10 g/kg body weight daily administration.[25] The human equivalent doses translated from the mouse study will be 0.4 and 0.8 g/kg daily, which could be difficult for long-term treatment in clinics. Further, ribitol, although being a natural metabolite, has not been consumed by humans, especially at the stated doses, and therefore potential side effects are unknown. Even though a dose-escalating study with a clinically applicable regimen is required to obtain minimal effective dose for clinic application, a better understanding of the pathway by which ribitol is converted to CDP-ribitol, the final substrate of FKRP, would be valuable for improving efficacy in clinical application. In the current study, we have investigated the contribution of an enzymatic factor (ISPD) and a metabolic factor (ribitol) to the expression of α-DG glycosylation, either separately or in combination. Our results demonstrated for the first time *in vivo* that overexpression of human ISPD can increase levels of CDP-ribitol in the absence and presence of an exogenous supply of ribitol and resulted in enhanced levels of F-α-DG in cardiac and skeletal muscle in the FKRP mutant mouse model. This result provides an encouraging prospect that modulation of other elements within the pathway leading to the synthesis of F-α-DG could also be explored to compensate for the reduced function of mutant FKRPs and achieve the desirable higher efficacy in combination with treatments such as ribitol supplement.

Consistent with our early report, the effect on levels of F-α-DG with ribitol treatment was tissue specific, being more pronounced in heart than in limb muscle or diaphragm. The mechanisms behind the tissue specificity is not fully understood. Interestingly, quantification analysis showed that levels of ribitol, especially ribitol-5P and CDP-ribitol, are clearly higher in heart compared with skeletal tissue. Therefore, variation in metabolism in a tissue-specific fashion could result in variable levels of different metabolites, including those involved in the synthesis of ribitol-5P and CDP-ribitol, affecting efficiency of either ribitol-induced or ISPD overexpression-induced F-α-DG. However, ribitol-mediated restoration of F-α-DG could also involve stabilization and turnover of the mutant FKRP protein, thus enhancing its function. This hypothesis deserves further investigation.

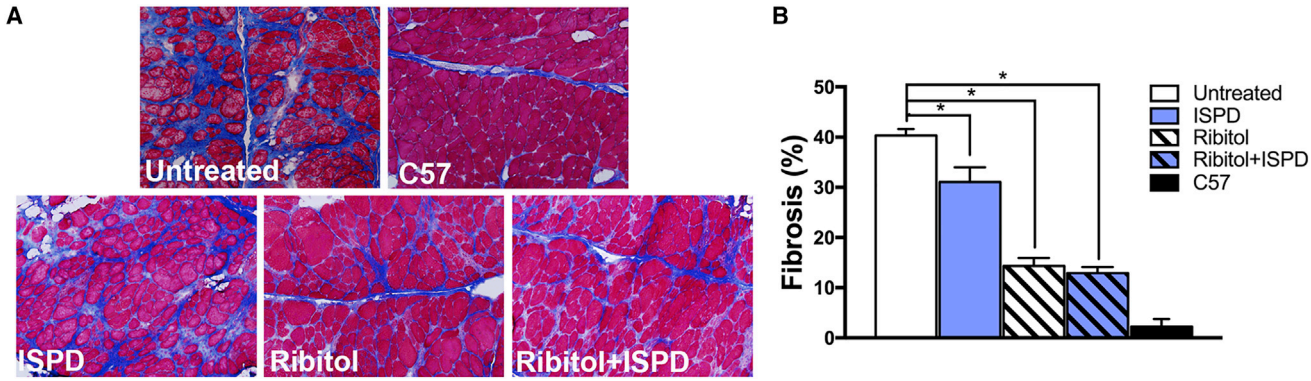

Figure 6. Effect of Exogenous ISPD and Ribitol on Fibrosis in Diaphragm of P448L Mice Treated for 6 Months

(A) Masson's Trichrome staining on diaphragm of untreated mice (drinking water only), mice treated with 5e13 vg/kg AAV9-ISPD (ISPD), and mice drinking water supplemented with 5% ribitol (Ribitol). Mice receiving combined treatment were injected with 5e13 vg/kg AAV9-ISPD and drank water supplemented with 5% ribitol (Ribitol + ISPD). Scale bar, 50 μm. (B) Percentage of fibrotic areas quantified from Masson's Trichrome staining shown in (A) (n = 4 per each cohort). Error bars represent mean ± SEM. Unpaired t test, *$p \leq 0.05$.

The most remarkable findings of the current study are the results from the combined therapeutic approach. We have demonstrated that the potential benefits of ribitol therapy could be enhanced by overexpressing ISPD in the presence of exogenous ribitol. Ribitol and ISPD act synergistically and can increase levels of F-α-DG up to 40% of normal values in cardiac tissue and more than 20% and 30% in limb and diaphragm, respectively. Importantly, the results of our work arise as a valid alternative to large-dose administration of ribitol, thus reducing potential side effects. Equally important, we have demonstrated that while supplying high doses of ribitol, equivalent to 5 g/kg body weight daily, the endogenous levels of ISPD become the limiting factor for the synthesis of CDP-ribitol. About four times more CDP-ribitol is synthesized from the exogenous ribitol when ISPD is overexpressed compared with the amount produced with the endogenous levels of ISPD in heart. This suggests that increasing efficiency rather than increasing dosage of ribitol could be further explored for higher efficacy.

Another interesting finding of the current study is the differential effect of ISPD overexpression on respiratory function over time. ISPD overexpression with 5e13 vg/kg AAV9 administration partially restores F-α-DG with clear improvement in limb muscle functions. An amelioration of the respiratory performance parameters was also observed at 3 months post-AAV9 treatment. However, the improvement is apparently reverted to statistically significant decline 6 months after the initiation of the treatment. The mechanism for this alteration is not understood. The reversal in these parameters was not observed in the ribitol-treated cohorts. Exogenous ISPD expression could therefore be responsible for this effect. Because the function of ISPD has been only recently identified, additional functions other than ribitol-5P transferase for F-α-DG cannot be excluded. Thus, potential side effects with ISPD overexpression over time require attention, and further studies will be necessary to consider ISPD as a candidate for gene therapy applicable to dystroglycanopathies.

MATERIALS AND METHODS

Animal Care

All animal studies were approved by the Institutional Animal Care and Use Committee (IACUC) of Carolinas Medical Center. All mice were housed in the vivarium of Carolinas Medical Center following animal care guidelines of the institute. Animals were ear tagged prior to group assignment. Food and water were available *ad libitum* during all phases of the study. Body weight was measured from 6 to 32 weeks of age.

Mouse Model

FKRP P448L mutant mice were generated by the McColl-Lockwood Laboratory for Muscular Dystrophy Research.[27,28] The mice contain a homozygous missense mutation (*c.1343C>T*, p.Pro448Leu) in the *FKRP* gene with the floxed neomycin-resistant (Neo^r) cassette removed from the insertion site. *C57BL/6* (wild-type/C57) mice were purchased from Jackson Laboratory.

AAV Vector and Ribitol Administration

The recombinant AAV9-ISPD vector was purchased from ViGene Biosciences (Rockville, MD, USA). ORF of human ISPD (GenBank: NM_002201426), transcript variant 1, and a C-terminal FLAG/His tag were cloned into the pAV-FH plasmid under control of a CMV promoter, which was later used to produce the AAV9-ISPD vector. Detailed information regarding vector production and purification can be found on the ViGene Biosciences website (http://www.vigenebio.com). The title of the stock virus was 4.73e14 genome copies/mL. AAV9-ISPD was given as a single tail-vein injection to 5-week-old *P448L* mice, either in a dose of 1e13 or 5e13 vg/kg diluted with saline to a final volume of 100 μL.

Ribitol was purchased from Sigma (A5502 Adonitol, ≥98%; Sigma, St. Louis, MO, USA) and dissolved in drinking water to

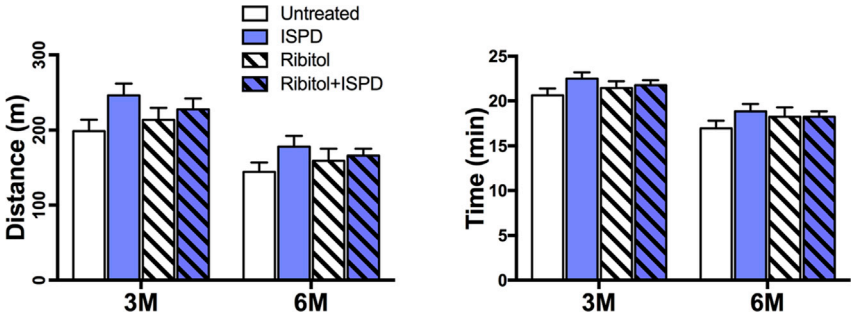

Figure 7. Effect of Ribitol and ISPD on Skeletal Muscle Function of P448L Mice

Treadmill exhaustion test assessing running distance (m) and time (min) in treated and age-matched untreated P448L mice. Test was performed at 3 and 6 months post-treatment (3M and 6M, respectively). Mice were injected with 5e13 vg/kg AAV9-ISPD (ISPD), drank water supplemented with 5% ribitol (Ribitol), or received combined treatment with 5e13 vg/kg AAV9-ISPD and 5% ribitol supplemented water (Ribitol + ISPD) (n = 12 and n = 6 per each cohort at 3- and 6-month time point, respectively). Error bars represent mean ± SEM. Unpaired t test, $p \leq 0.05$.

the final concentration of 5%. *P448L* mice aged 7 weeks were treated with 5% ribitol drinking water for 3 and 6 months. All of the mice were randomly assigned to either treatment or control groups. A minimum number of six mice was used for each group. No animal was excluded. Untreated age-matched *P448L* and wild-type *C57BL/6* mice were used as controls. The animals were terminated at the end of each treatment time point, and tissues including heart, diaphragm, TA, and quadriceps were collected for analyses.

Immunohistochemical and Western Blot Analysis

Tissues were dissected and snap-frozen in dry-ice-chilled 2-methylbutane. For immunohistochemical detection of functionally glycosylated α-DG, 6-μm-thick cross sections of untreated and *C57* control, as well as tissues from treated cohorts, were included in each slide. Slides were first fixed in ice-cold ethanol:acetic acid (1:1) for 1 min, blocked with 10% normal goat serum (NGS) in 1× Tris-buffered saline (TBS) for 30 min at room temperature, and incubated overnight at 4°C with primary mouse monoclonal antibody IIH6C4 (05-593, 1:500; EMD Millipore) against F-α-DG. Negative controls received 10% NGS in 1× TBS only. Sections were washed and incubated with secondary Alexa Fluor 488 goat anti-mouse immunoglobulin M (IgM; A-21042, 1:500; Invitrogen) at room temperature for 2 h. Sections were washed and finally mounted with fluorescence mounting medium (Dako) containing 1× DAPI (4′,6′-diamidino-2-phenylindole) for nuclear staining. Immunofluorescence was visualized using an Olympus BX51/BX52 fluorescence microscope (Opelco), and images were captured using the Olympus DP70 digital camera system (Opelco). Slides were examined in a blinded manner by the investigator.

For western blot analysis, tissues were homogenized in extraction buffer (50 mM Tris-HCl [pH 8.0], 150 mM NaCl, and 1% Triton X-100), supplemented with 1× protease inhibitor cocktail (Sigma-Aldrich). Protein concentration was quantified by the Bradford assay (DC protein assay; Bio-Rad). A total of 50 μg of protein was loaded on a 4%–15% Bio-Rad Mini-PROTEAN TGX gel (Bio-Rad) and immunoblotted. The amount of total protein loaded for *C57* mice was half of the amount loaded for the *P448L* mice. Nitrocellulose membranes (Bio-Rad) were blocked with 5% milk in 1× phosphate-buffered saline (PBS) for 2 h at room temperature and then incubated with the following primary antibodies overnight at 4°C: IIH6C4 (1:2,000), FLAG-Tag (DYKDDDDK) (Invitrogen) (1:500), and α-actin (Sigma) (1:1,000). Appropriate horseradish peroxidase (HRP)-conjugated secondary antibodies were incubated for 2 h at room temperature. All blots were developed by electrochemiluminescence immunodetection (PerkinElmer). For IIH6C4 band quantification from western blot, ImageJ software was used. For laminin overlay assay, nitrocellulose membranes were blocked with laminin overlay buffer (10 mM ethanolamine, 140 mM NaCl, 1 mM $MgCl_2$, and 1 mM $CaCl_2$ [pH 7.4]) containing 5% nonfat dry milk for 1 h at 4°C, followed by incubation with laminin from Engelbreth-Holm-Swarm murine sarcoma basement membrane (L2020; Sigma) at a concentration of 2 μg/mL overnight at 4°C in laminin overlay buffer. Membranes were then incubated with rabbit anti-laminin antibody (L9393, 1:1,500; Sigma), followed by goat anti-rabbit HRP-conjugated IgG secondary antibody (1:3,000; Santa Cruz Biotechnology). Blots were saturated with Western-Lightning Plus ECL (Perkin-Elmer) before exposure to and developing of GeneMate auto-radiographic film (VWR).

Histopathological and Morphometric Analysis

Frozen tissues were processed for H&E and Masson's Trichrome staining following standard procedures. Muscle cross-sectional fiber-equivalent diameter was determined from tibialis anterior stained with H&E using MetaMorph v7.7 Software (Molecular Devices). The percentage of centrally nucleated myofibers was manually quantified from the same tissue sections stained with H&E. Fibrotic area represented by blue staining in the Masson's Trichrome-stained sections was quantified from diaphragm using the ImageJ software. For all of the morphometric analyses, a total of 500–600 fibers from four representative ×20 magnification images per each muscle per animal was used.

Quantitative Reverse Transcriptase PCR Assay

Tissues were collected from heart, diaphragm, and tibialis anterior. RNA was extracted using TRIzol (Invitrogen) following the supplied protocol. Final RNA pellet was re-suspended in 20 μL RNase-nuclease-free water. Final RNA concentration was determined using NanoDrop 2000c. One microgram of RNA was subsequently converted to complementary DNA (cDNA) using the High-Capacity RNA-to-cDNA Kit (Applied Biosystems) following the supplied protocol. cDNA was then used for quantitative real-time PCR using the mouse FKRP-FAM (Mm00557870_m1) TaqMan gene expression assay with primer limited GAPDH-VIC (Mm99999915_g1) as the

internal control (Thermo Fisher Scientific) and TaqMan Universal Master Mix II, with UNG (Life Technologies). Quantitative real-time PCR was run on the Bio-Rad CFX96 Touch Real-Time PCR Detection System (Bio-Rad) following the standard real-time PCR conditions suggested for TaqMan assays. Results of FKRP transcript were calculated and expressed as $2^{-\Delta\Delta Ct}$, and compared across tissues and animals.

Metabolite Extraction from Muscle Tissues and LC/MS-MS Analysis

Ribitol was purchased from Sigma (A5502). Ribitol-5P and CDP-ribitol were synthesized by Z-Biotech (Aurora, CO, USA). Muscle tissues were collected, and blinded samples were subjected to the following procedure. Thirty to eighty micrograms of frozen tissue samples was homogenized with 400 μL MeOH:acetonitrile (ACN) (1:1) and then centrifugated for 5 min at 8,000 × *g*. The supernatants were removed, transferred to individual wells of a 96-well plate, and analyzed by LC/MS-MS. An Applied Biosystems Sciex 4000 (Applied Biosystems, Foster City, CA, USA) equipped with a Shimadzu HPLC (Shimadzu Scientific Instruments, Columbia, MD, USA) and Leap auto-sampler (LEAP Technologies, Carrboro, NC, USA) was used to detect ribitol, ribitol-5P, and CDP-ribitol from tissue samples and synthetic compounds. The metabolites were separated on a silica gel column (Hypersil Silica 250 × 4.6 mm, 5-μm particle size) using solvent A (water, 10 mM NH_4OAc, 0.1% formic acid) and solvent B (MeOH:ACN [1:1]). The following gradient was used: 0–12 min, 5% buffer B; 13–14 min, 95% buffer B; 15–17 min, 5% buffer B. Under these conditions, ribitol, ribitol-5P, and CDP-ribitol eluted at 8.3, 7.5, and 8.9 min, respectively. The metabolites were analyzed using electrospray ionization mass spectrometry operated in positive ion mode, ESI+. The compounds concentrations in tissue samples were determined based on standard curves prepared by serial dilutions (200 to 0.01 μM) of each of the compounds in MeOH:ACN (1:1).

Muscle Function Tests

For the treadmill exhaustion test, 17- and 30-week-old mice were placed on the belt of a five-lane motorized treadmill (LE8700 treadmill; Panlab/Harvard Apparatus, Barcelona, Spain) supplied with shock grids mounted at the back of the treadmill, which delivered a 0.2-mA current to provide motivation for exercise. Initially, the mice were subjected to an acclimation period (time, 5 min; speed, 8 cm/s, and 0° incline). Immediately after the acclimation period, the test commenced with speed increases of 2 cm/s every minute until exhaustion. The test was stopped and the time to exhaustion was determined when the mouse remained on the shock grid for 5 s without attempting to re-engage the treadmill.[15]

Whole-Body Plethysmography

Respiratory functional analysis in conscious, freely moving, 18- and 31-week-old mice was measured using a whole-body plethysmography technique as described previously.[15] The plethysmograph apparatus (emka Technologies, Falls Church, VA, USA) was connected to a ventilation pump to maintain a constant air flow, a differential pressure transducer, a usbAMP signal amplifier, and a computer running EMKA iox2 software with the respiratory flow analyzer module, which was used to detect pressure changes caused by breathing and recording the transducer signal. An initial amount of 20 mL of air was injected and withdrawn via a 20-mL syringe into the chamber for calibration. Mice were placed inside the free-moving plethysmograph chamber and allowed to acclimate for 5 min to minimize any effects of stress-related changes in ventilation. Resting ventilation was measured for a duration of 15 min after the acclimation period. Body temperatures of all mice were assumed to be 37°C and to remain constant during the ventilation protocol.

Statistical Analysis

All data are expressed as mean ± SEM unless stated otherwise. Statistical analyses were performed with GraphPad Prism version 7.01 for Windows (GraphPad Software). Individual means were compared using multiple t tests. Statistical significance was determined using the Holm-Sidak method to correct for multiple comparisons, with alpha = 0.05.

Data Availability

The authors declare that all data supporting the findings of this study are available within the article and its Supplemental Information.

SUPPLEMENTAL INFORMATION

Supplemental Information can be found online at https://doi.org/10.1016/j.omtm.2019.12.005.

AUTHOR CONTRIBUTIONS

Conceptualization, M.P.C. and Q.L.L.; Methodology, M.P.C. and Q.L.L.; Validation, M.P.C.; Formal Analysis, M.P.C.; Investigation, M.P.C., A.B., P.L., and V.L.; Resources, Q.L.L.; Data Curation, M.P.C.; Writing – Original Draft, M.P.C.; Writing – Review & Editing, M.P.C., A.B., and Q.L.L.; Visualization, M.P.C.; Supervision, Q.L.L.; Project Administration, M.P.C. and Q.L.L.; Funding Acquisition, Q.L.L.

CONFLICTS OF INTEREST

The authors declare no competing interests.

ACKNOWLEDGMENTS

This work was supported by the Carolinas Muscular Dystrophy Research Endowment at the Atrium Health Foundation. The authors thank Brooke King and Natalia Zinchenko (James G. Cannon Research Center Core Histology Laboratory at Carolinas Medical Center) for assistance with histological staining, and the vivarium staff (James G. Cannon Research Center Vivarium at Carolinas Medical Center) for caring for the animals.

REFERENCES

1. Kanagawa, M., and Toda, T. (2006). The genetic and molecular basis of muscular dystrophy: roles of cell-matrix linkage in the pathogenesis. J. Hum. Genet. *51*, 915–926.

2. Ervasti, J.M., and Campbell, K.P. (1991). Membrane organization of the dystrophin-glycoprotein complex. Cell *66*, 1121–1131.

3. Ervasti, J.M., and Campbell, K.P. (1993). A role for the dystrophin-glycoprotein complex as a transmembrane linker between laminin and actin. J. Cell Biol. *122*, 809–823.

4. Gee, S.H., Montanaro, F., Lindenbaum, M.H., and Carbonetto, S. (1994). Dystroglycan-alpha, a dystrophin-associated glycoprotein, is a functional agrin receptor. Cell *77*, 675–686.

5. Talts, J.F., Andac, Z., Göhring, W., Brancaccio, A., and Timpl, R. (1999). Binding of the G domains of laminin alpha1 and alpha2 chains and perlecan to heparin, sulfatides, alpha-dystroglycan and several extracellular matrix proteins. EMBO J. *18*, 863–870.

6. Sugita, S., Saito, F., Tang, J., Satz, J., Campbell, K., and Südhof, T.C. (2001). A stoichiometric complex of neurexins and dystroglycan in brain. J. Cell Biol. *154*, 435–445.

7. Yoshida-Moriguchi, T., and Campbell, K.P. (2015). Matriglycan: a novel polysaccharide that links dystroglycan to the basement membrane. Glycobiology *25*, 702–713.

8. Brockington, M., Blake, D.J., Prandini, P., Brown, S.C., Torelli, S., Benson, M.A., Ponting, C.P., Estournet, B., Romero, N.B., Mercuri, E., et al. (2001). Mutations in the fukutin-related protein gene (FKRP) cause a form of congenital muscular dystrophy with secondary laminin alpha2 deficiency and abnormal glycosylation of alpha-dystroglycan. Am. J. Hum. Genet. *69*, 1198–1209.

9. Beltran-Valero de Bernabé, D., Voit, T., Longman, C., Steinbrecher, A., Straub, V., Yuva, Y., Herrmann, R., Sperner, J., Korenke, C., Diesen, C., et al. (2004). Mutations in the FKRP gene can cause muscle-eye-brain disease and Walker-Warburg syndrome. J. Med. Genet. *41*, e61.

10. Michele, D.E., Barresi, R., Kanagawa, M., Saito, F., Cohn, R.D., Satz, J.S., Dollar, J., Nishino, I., Kelley, R.I., Somer, H., et al. (2002). Post-translational disruption of dystroglycan-ligand interactions in congenital muscular dystrophies. Nature *418*, 417–422.

11. Mercuri, E., Brockington, M., Straub, V., Quijano-Roy, S., Yuva, Y., Herrmann, R., Brown, S.C., Torelli, S., Dubowitz, V., Blake, D.J., et al. (2003). Phenotypic spectrum associated with mutations in the fukutin-related protein gene. Ann. Neurol. *53*, 537–542.

12. Mercuri, E., Topaloglu, H., Brockington, M., Berardinelli, A., Pichiecchio, A., Santorelli, F., Rutherford, M., Talim, B., Ricci, E., Voit, T., and Muntoni, F. (2006). Spectrum of brain changes in patients with congenital muscular dystrophy and FKRP gene mutations. Arch. Neurol. *63*, 251–257.

13. Brown, S.C., Torelli, S., Brockington, M., Yuva, Y., Jimenez, C., Feng, L., Anderson, L., Ugo, I., Kroger, S., Bushby, K., et al. (2004). Abnormalities in alpha-dystroglycan expression in MDC1C and LGMD2I muscular dystrophies. Am. J. Pathol. *164*, 727–737.

14. Wu, B., Shah, S.N., Lu, P., Richardson, S.M., Bollinger, L.E., Blaeser, A., Madden, K.L., Sun, Y., Luckie, T.M., Cox, M.D., et al. (2016). Glucocorticoid Steroid and Alendronate Treatment Alleviates Dystrophic Phenotype with Enhanced Functional Glycosylation of α-Dystroglycan in Mouse Model of Limb-Girdle Muscular Dystrophy with FKRPP448L Mutation. Am. J. Pathol. *186*, 1635–1648.

15. Vannoy, C.H., Xiao, W., Lu, P., Xiao, X., and Lu, Q.L. (2017). Efficacy of Gene Therapy Is Dependent on Disease Progression in Dystrophic Mice with Mutations in the FKRP Gene. Mol. Ther. Methods Clin. Dev. *5*, 31–42.

16. Vannoy, C.H., Leroy, V., and Lu, Q.L. (2018). Dose-Dependent Effects of FKRP Gene-Replacement Therapy on Functional Rescue and Longevity in Dystrophic Mice. Mol. Ther. Methods Clin. Dev. *11*, 106–120.

17. Kanagawa, M., Kobayashi, K., Tajiri, M., Manya, H., Kuga, A., Yamaguchi, Y., Akasaka-Manya, K., Furukawa, J.I., Mizuno, M., Kawakami, H., et al. (2016). Identification of a Post-translational Modification with Ribitol-Phosphate and Its Defect in Muscular Dystrophy. Cell Rep. *14*, 2209–2223.

18. Gerin, I., Ury, B., Breloy, I., Bouchet-Seraphin, C., Bolsée, J., Halbout, M., Graff, J., Vertommen, D., Muccioli, G.G., Seta, N., et al. (2016). ISPD produces CDP-ribitol used by FKTN and FKRP to transfer ribitol phosphate onto α-dystroglycan. Nat. Commun. *7*, 11534.

19. Riemersma, M., Froese, D.S., van Tol, W., Engelke, U.F., Kopec, J., van Scherpenzeel, M., Ashikov, A., Krojer, T., von Delft, F., Tessari, M., et al. (2015). Human ISPD Is a Cytidyltransferase Required for Dystroglycan O-Mannosylation. Chem. Biol. *22*, 1643–1652.

20. Praissman, J.L., Willer, T., Sheikh, M.O., Toi, A., Chitayat, D., Lin, Y.Y., Lee, H., Stalnaker, S.H., Wang, S., Prabhakar, P.K., et al. (2016). The functional O-mannose glycan on α-dystroglycan contains a phospho-ribitol primed for matriglycan addition. eLife *5*, e14473.

21. Cirak, S., Foley, A.R., Herrmann, R., Willer, T., Yau, S., Stevens, E., Torelli, S., Brodd, L., Kamynina, A., Vondracek, P., et al.; UK10K Consortium (2013). ISPD gene mutations are a common cause of congenital and limb-girdle muscular dystrophies. Brain *136*, 269–281.

22. Willer, T., Lee, H., Lommel, M., Yoshida-Moriguchi, T., de Bernabe, D.B., Venzke, D., Cirak, S., Schachter, H., Vajsar, J., Voit, T., et al. (2012). ISPD loss-of-function mutations disrupt dystroglycan O-mannosylation and cause Walker-Warburg syndrome. Nat. Genet. *44*, 575–580.

23. Roscioli, T., Kamsteeg, E.J., Buysse, K., Maystadt, I., van Reeuwijk, J., van den Elzen, C., van Beusekom, E., Riemersma, M., Pfundt, R., Vissers, L.E., et al. (2012). Mutations in ISPD cause Walker-Warburg syndrome and defective glycosylation of α-dystroglycan. Nat. Genet. *44*, 581–585.

24. Tasca, G., Moro, F., Aiello, C., Cassandrini, D., Fiorillo, C., Bertini, E., Bruno, C., Santorelli, F.M., and Ricci, E. (2013). Limb-girdle muscular dystrophy with α-dystroglycan deficiency and mutations in the ISPD gene. Neurology *80*, 963–965.

25. Cataldi, M.P., Lu, P., Blaeser, A., and Lu, Q.L. (2018). Ribitol restores functionally glycosylated α-dystroglycan and improves muscle function in dystrophic FKRP-mutant mice. Nat. Commun. *9*, 3448.

26. Zincarelli, C., Soltys, S., Rengo, G., and Rabinowitz, J.E. (2008). Analysis of AAV serotypes 1-9 mediated gene expression and tropism in mice after systemic injection. Mol. Ther *16*, 1073–1080.

27. Chan, Y.M., Keramaris-Vrantsis, E., Lidov, H.G., Norton, J.H., Zinchenko, N., Gruber, H.E., Thresher, R., Blake, D.J., Ashar, J., Rosenfeld, J., and Lu, Q.L. (2010). Fukutin-related protein is essential for mouse muscle, brain and eye development and mutation recapitulates the wide clinical spectrums of dystroglycanopathies. Hum. Mol. Genet. *19*, 3995–4006.

28. Blaeser, A., Keramaris, E., Chan, Y.M., Sparks, S., Cowley, D., Xiao, X., and Lu, Q.L. (2013). Mouse models of fukutin-related protein mutations show a wide range of disease phenotypes. Hum. Genet. *132*, 923–934.